Rhenium carbonyl complexes conjugated with methylated triphenylphosphonium cations as sensitive mitochondria trackers for X-ray fluorescence imaging

Gabrielle Schanne,[a] Lucas Henry,[a] How Chee Ong,[b] Andrea Somogyi,[c] Kadda Medjoubi,[c] Nicolas Delsuc,[a] Clotilde Policar,[a] Felipe García,[b*] Helene C. Bertrand[a,b*]

[a]Laboratoire des biomolécules, LBM, Département de chimie, Ecole normale supérieure, PSL University, Sorbonne université, CNRS, 75005 Paris, France.
E-mail: helene.bertrand@ens.psl.eu
[b] School of Physical and Mathematical Sciences, Division of Chemistry and Biological Chemistry, Nanyang Technological University, 21 Nanyang Link, 637371, Singapore
E-mail: fgarcia@ntu.edu.sg
[c] Synchrotron SOLEIL, BP 48, Saint-Aubin, 91192 Gif sur Yvette, France

Abstract

Synchrotron Radiation X-ray Fluorescence (SXRF) imaging is a powerful technique for the visualization of metal complexes in biological systems. However, due to the lack of an endogenous elemental signature for mitochondria, probes for the localization of this organelle are required for colocalization studies. In this work, we designed and synthesized rhenium pyta tricarbonyl complexes conjugated to methylated triphenylphosphonium TP*P$^+$ cations as multimodal probes for the visualization of mitochondria, suitable for fluorescence and SXRF imaging and quantification. Accumulation of the methylated triphenylphosphonium TP*P$^+$-based conjugates in cells was observed in fixed A549 cells, and the amount of mitochondrial uptake was linked to the lipophilicity of the TPP$^+$ vector. Our work highlights a convenient rhenium-based multimodal mitochondrial-targeted probe compatible with SXRF nano-imaging.

Introduction

The subcellular detection, localization, and quantification of small molecules in cellular medium and in particular of transition metal complexes are crucial in their development in biology and medicine and in the understanding of their biological mode of action. Several methods can be used to study the subcellular localization of a compound of interest: study of pharmacological effects, chemical analysis and the most widely employed microscopic imaging studies using spectroscopic probes specific for individual organelles.[1] Among the common approaches, fluorescence microscopy using fluorescent probes is pivotal as a non-invasive imaging technique for its convenience, good sensitivity and high spatial resolution, resulting in the routine use of organelle-specific fluorophores as conventional markers in fluorescence imaging.[2-4] Despite their popularity and utility, fluorescent probes still suffer

from some drawbacks such as photobleaching and limited laser penetration depths. Moreover, fluorescence imaging is dependent on environmental factors such as medium polarity, pH, binding status, *etc.*, that can modify the quantum yield and/or emission spectrum, possibly rendering apparent subcellular distribution inaccurate.[5-6] More importantly, the commonly used strategy of appending a large organic fluorophore on a non-fluorescent compound of interest to enable its detection may modify its molecular parameters and hence alter subcellular distribution.[7-8]

The developments of imaging techniques and organelle-specific probes based on complementary modalities are hence of primary importance. In the context of metal imaging, X-ray fluorescence (XRF) nano-imaging is highly promising as it allows for the specific and direct imaging of the metal centre. Hard X-ray scanning XRF spectroscopy enables the simultaneous mapping of all elements having Z>14 provided their edge energy is lower than the incident X-ray energy. Thus, information on both the chemical environment and the studied metal centre's distribution in biological environments and cells[9] is readily available. Using highly focalised synchrotron beams, resolutions as good as a few 10 nm's can be obtained. Moreover, scanning Synchrotron Radiation X-ray Fluorescence (SXRF) imaging has a high analytical sensitivity (≤ ppm). SXRF spectroscopy thus exhibits a high detection sensitivity, a high specificity and a high spatial resolution. SXRF nano-imaging in studies of metallodrugs have received increasing attention in the last decade[10-15] and provided valuable information on the fate of the metal complexes in the cellular context. XRF imaging is, hence, highly promising as a tool in the growing field of inorganic medicinal chemistry.

For co-localization studies by XRF, some endogenous elements can be indicative of a subcellular compartment – *e.g*. phosphorus and zinc reveal nucleus localization,[16] while manganese has been shown to accumulate in the Golgi apparatus in neural cells – [17] although this is not the case for all the organelles. 3D XRF nano-imaging was recently used to determine the subcellular localization of anticancer metal complexes.[18-19] Sealed carbon nanotubes filled with heavy metals and decorated with organelle-specific peptides were described for the XRF mapping of cell membrane, nucleus and endoplasmic reticulum.[20] Mitochondria localization, up to now, has only been identified by XRF using correlative imaging with fluorescence[21] or electron microscopy[22] or using an immunolabeling technique

involving a secondary antibody functionalized with gold nanoparticles.[23-24] Hence, systems of easier access such as low molecular weight XRF imaging molecular probes with specific organelle targeting in the manner of conventional fluorophores, with an additional modality such as classical fluorescence for validation, would be highly valuable tools for colocalization studies and convenient access to the accurate localization of metal complexes by XRF.

One promising system for that purpose is multimodal rhenium(I) carbonyl-based probes, that can be visualized through infrared (IR), fluorescence and XRF imaging. These biologically-stable octahedral d^6 low-spin Re(I) tricarbonyl complexes, of general formula $[Re(CO)_3(N^N)X]$ (with N^N a diimine ligand with low-energy π* orbitals), show exciting and valuable photophysical properties such as low toxicity, large Stokes shifts and long luminescent lifetimes that render them suitable for bio-imaging.[25-27] These complexes have thus been developed to target different cell compartments as luminescent organelle trackers as described in recent reviews.[28-29] $Re(CO)_3$ complexes also display IR absorptions in the range 1800-2200 cm^{-1}, a spectral region in which biological media are transparent. This combination of properties enables the use of these complexes as Single Core Multimodal Probe for Imaging (SCoMPI) in cells and tissues,[30-33] while the IR signature of the complexes enabled their quantification inside cells, [5] as demonstrated in correlative fluorescence and infrared imaging studies. Most notably, these $Re(CO)_3$ complexes can also be mapped by XRF nano-imaging, as recently demonstrated.[12, 34-35] Rhenium is highly suitable for this function as it is highly emissive in X-fluorescence (after irradiation at > 12.53 keV), and its natural abundance is very low (ultra-trace element in urine and plasma (< 1 μg/g)),[36] leading to a good signal-to-noise ratio.

Ideally, to exert their biological effect, compounds must reach their subcellular targets while reducing accumulation in non-targeted sites to reduce associated side effects. There is therefore a high interest in drug targeting strategies to direct a compound to its specific site of action.[37-38, 39] One of such targets that have recently drawn attention has been mitochondria organelle due to its increasing association with metabolic diseases and neurodegenerative diseases *inter alia*.[40-42] To confer mitochondrial selectivity,[43-44] lipophilic cations such as mitochondrial-targeting peptides (MTPs)[45-47] or triphenylphosphonium (TPP^+)[48-49] derivatives can be conjugated to the cargo of interest, thus exploiting the mitochondrion's strong negative potential (up to 180–200 mV), allowing accumulation

within the mitochondrial matrix according to the Nernst equation.[50] In this context, the triphenylphosphonium (TPP^+) moiety – which is the "gold standard" among mitochondrial delivery vectors – has been broadly used as a molecular vector for selective mitochondrial delivery owing to its high lipophilicity, cationic nature, high stability in physiological conditions and its ease of conjugation to molecular cargo.[49] The versatility of this platform is exemplified by the wide range of molecules that has been delivered into the mitochondria through TPP^+ conjugation, such as spin-traps, antioxidants, prodrugs, protonophores, fluorophores, photodynamic therapy sensitizers as well as positron emitters.[49]

Although metal-based probes – mainly Ir(III), Ir(I) and Ru(II)[51] and a handful of $Re(CO)_3$ complexes[52-55] – have been described to target mitochondria, to the best of our knowledge, none were used as molecular probes in XRF imaging. As mentioned above, the techniques used so far require the most advanced 3D XRF progresses or immunolabeling techniques that could be cumbersome. Finally, there is no XRF-detectable endogenous and ubiquitous element characteristic for the mitochondria, making a mitochondria targeting XRF probe of particular interest.

In light of the need for an organelle-specific multimodal probe compatible with XRF techniques, we have designed and synthesized three triarylphosphonium-$[Re(CO)_3(pyta)X]$ mitochondria-targeted probes suitable for X-fluorescence mapping and quantification. We explored methylated TPP derivatives (i.e., TP^*P^+) that were shown in recent studies to display enhanced performance as compared to the conventionally used TPP^+ moiety. For instance, TP^*P^+ species have shown a two-fold performance enhancement in *in-vitro* photodynamic therapy (PDT) studies, and have also enabled the accumulation of dicationic species previously described as unable to permeate the mitochondrial membrane.[56-57] The increase in lipophilicity by enhancement of the molecular volume and solvent accessible surface area (SASA) of the cations was proposed as key determinant to improve mitochondria accumulation.[56-57]

Here, we report the synthesis of a series of rhenium pyta tricarbonyl complexes conjugated to triarylphosphonium cations. Toxicity and imaging studies were performed in A549 cells, revealing lipophilicity-dependent toxicity associated with increasing internalization of the compounds. Mitochondria localization was assessed by colocalization studies in fluorescence

imaging using a conventional mitochondria stain Mitotracker Deep Red. Subcellular XRF mapping of the compounds was successfully achieved by SXRF imaging using the Re-Lß edge of Re. We describe here the conjugate with the bis-methyl TP*P$^+$ cation **C3** as a low toxicity mitochondria-targeted metal-based multimodal probe that can be mapped and quantified inside cells using SXRF. Our study confirms the potential of methyl functionalized TPP$^+$ as mitochondrial delivery vectors with enhanced properties.

Synthesis

We synthesized conjugates **C1-3** comprising three triphenylphosphonium cation derivatives with a rhenium pyta tricarbonyl complex[58-60] based respectively on the classical TPP$^+$ cation (R^m = R^p = H), the modified TP*P$^+$ cation bearing a methyl group on phenyl *para* positions (R^m = H, R^p = Me) and the modified TP*P$^+$ cation bearing methyl groups on all phenyl *meta* positions (R^m = Me, R^p = H) (Scheme 1). A beta-alanine spacer was chosen to bridge the pyta ligand with the aminoethyl phosphonium cations. Increasing the alkyl chain length between the cargo and the TPP$^+$ cation vector is known to increase the cell penetration of the construct.[61-63] For practical reasons in the synthesis and consistent data interpretation, we chose to keep the spacer constant and only the nature of the phosphonium vector was changed.

Therefore, β-Alanine *tert*-butyl ester hydrochloride was first reacted with chloroacetyl chloride in the presence of diisopropylethylamine (DIEA) in dichloromethane (Scheme 1, step i). Chloride nucleophilic substitution with sodium azide followed by a copper catalyzed azide alkyne cycloaddition (CuAAC) using copper sulfate pentahydrate and sodium ascorbate with ethynyl pyridine generated the pyridine-triazole (pyta) ligand functionalized with a *tert*-butyl ester terminated linker **3** (steps ii-iii).[34] The corresponding rhenium carbonyl complex **4** was obtained by reaction with rhenium pentacarbonyl chloride in toluene under heating (step iv). Hydrolysis of the ester function was performed at this stage by treatment in a mixture of TFA in DCM, followed by treatment with concentrated HCl to afford a complex **5** with a chloride as unique X ligand (step v). The conjugates **C1-3** were finally obtained *via* an amide coupling with aminoethylphosphonium bromide derivatives **P1-3** prepared as previously described[56] using HOBt and EDC.HCl as coupling agents in the presence of DIEA in DMF (step vi).

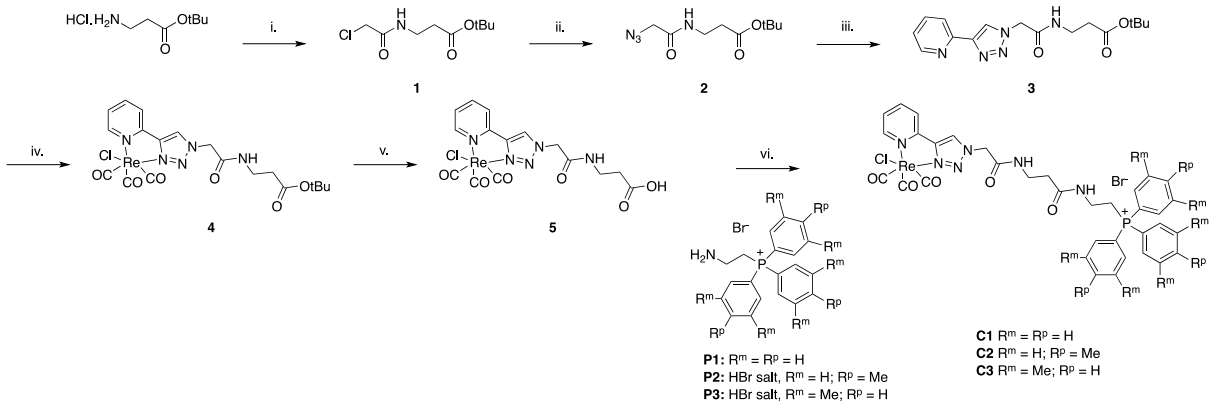

Scheme 1. Synthesis of conjugates **C1-3**. Conditions: i. chloroacetyl chloride (1.0 eq.), DIEA (2.5 eq.), DCM, 1 h, 25 °C (quantitative); ii. NaN_3 (1.97 eq.), NaI (0.1 eq.), acetone/H_2O 3:1 v:v, 17 h, 50 °C (89 %); iii. 2-ethynylpyridine (1.2 eq.), $CuSO_4.5H_2O$ (0.26 eq.), sodium ascorbate (1.0 eq.), acetone/H_2O 2:1 v:v, 2h, 25 °C (85%); iv. $Re(CO)_5Cl$ (1.1 eq.), toluene, 5 h, 80 °C (99%); v. TFA/DCM 1:1 v:v, 1 h, 25 °C then conc. HCl, 10 min, 25 °C (86 %); vi. (2-aminoethyl)triphenylphosphonium bromide derivative **P1-3** (1.1 eq.), HOBt (1.5 eq.), EDC.HCl (1.5 eq.), DMF, 24-48 h (20-70 %).

Photophysical properties

The photophysical properties of the conjugates **C1-3** were characterized in acetonitrile and are summarized in Table 1 and Figure S1. The three conjugates show typical absorptions of rhenium carbonyl complexes with a MLCT band centered at 330 nm in acetonitrile (Figure S1).[5, 58, 60] Excitation at 330 nm led to a broad emission band centered at 530 nm. **C1-3** showed similar low quantum yields around 0.25-0.27%, consistent with rhenium carbonyl complexes with substitutions of comparable features.[58, 64]

Table 1. Photophysical properties of conjugates **C1-3** in acetonitrile and IC_{50} from MTT assay.

Complex	Excitation (nm)	Emission (nm)	Range (nm)	Quantum yield[a] (%)	IC_{50}	Hydrophobicity as per rt in RP-HPLC (min)
C1	330	530	450 - 620	0.27	413 ± 65	6.40
C2	330	530	450 - 620	0.27	100 ± 26	7.93
C3	330	530	450 - 620	0.25	46 ± 10	8.52

[a] Quinine sulfate in 0.1 N sulfuric acid was used as a standard with a known quantum yield of 54.6% (λ_{exc} 320 nm).

Toxicity

The toxicity of the conjugates was evaluated in A549 non-small cell lung cancer cell line using a classical 3-(4, 5-dimethylthiazol-2-yl)-2, 5-diphenyl tetrazolium bromide (MTT) assay.

The cells were incubated with a range of concentrations (1-1000 μM) for 4 h. The conjugates showed differential toxicity with IC_{50} comprised between 46 ± 10 μM for **C3** and 413 ± 65 μM for **C1** (Table 1, Figure S2-S3). The higher toxicity with increasing methyl functionalization of the phenyl rings of the phosphonium targeting moieties (**C1** to **C3**, with **C3** 10 times more cytotoxic than **C1**) is consistent with an increased hydrophobicity, as supported by the increased retention time in reverse phase analytical HPLC (6.40, 7.93, 8.52 min for **C1**, **C2**, and **C3**, respectively). This may be, in turn, consistent with a greater cell penetration. The viability at 10 μM and 20 μM, concentrations used for the subsequent imaging experiments, were > 80% for the three conjugates, and the slight toxicity observed at these concentrations did not preclude the imaging studies. Consequently, imaging studies using fluorescence and X-ray fluorescence spectroscopy were then performed to investigate the conjugates' sub-cellular localisation and quantify their accumulation in A549 cells.

Fluorescence imaging

A549 cells were incubated with 10 μM or 20 μM of the conjugates **C1-C3** for 4 h, fixed with 4% PFA and imaged by single photon excitation at 350 nm (Figure 1 and Figures S4-S7). For all the conjugates, a significant fluorescence signal was detected and localized around the nucleus. Mitochondrial labeling was then investigated using co-incubation with a conventional mitochondrial marker, MitoTracker Deep Red, characterized by an excitation maximum at 644 nm and an emission in the 650-750 nm range. The use of Mitotracker green (excitation 490 nm, emission 516 nm) as alternative mitochondria stain was not compatible with the $Re(CO)_3$ conjugates. During the imaging studies, a loss in intensity of the luminescence signal detected for the three conjugates **C1-C3** was observed when coincubated with MitoTracker Deep Red. Further studies in solution (see SI, Figure S8) showed that, although there is no overlap in the excitation spectra of the conjugates and the Mitotracker, there is a partial overlay between the emission of the conjugates (450-650 nm, centered at 530 nm in water) and the excitation of the organic fluorophore. An enhancement of Mitotracker fluorescence signal, along with a loss in luminescence signal of **C3** (λ_{exc} 320 nm) was consistently observed with an increasing concentration of Mitotracker. (SI Figure S9-S11). This suggests the existence of a fluorescence resonance energy transfer (FRET) between the two compounds, implying in turn, that the conjugates and the Mitotracker are in close proximity in cells, since FRET is distance-dependent. Despite this

intensity loss, the luminescence of the conjugates could still be detected without parasite signal (excitation of the Mitotracker at the excitation wavelength of the conjugates leads to a fluorescence signal (Figure S10) that is filtered out with a filter cut-off above 600 nm) and, the complexes sharing the same photophysical properties, the FRET phenomenon is expected to occur to the same extent, allowing us to qualitatively compare the cellular luminescence images in all three cases. Co-localization results were analyzed using the Van Steensel curve and Pearson value methods between the labeling of **C1-C3** and Mitotracker Deep Red in cells.

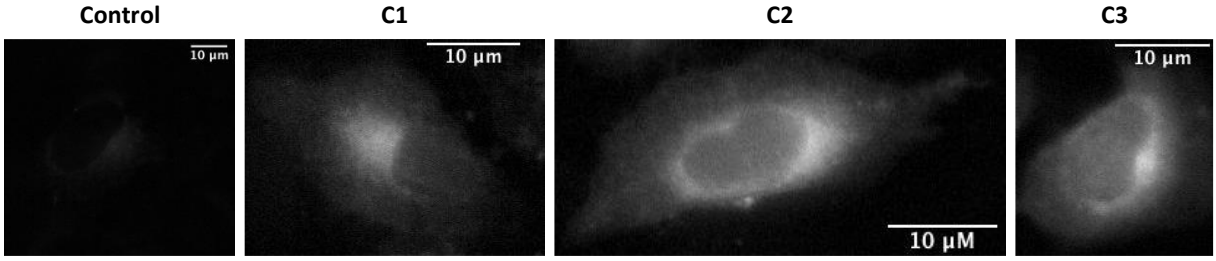

Figure 1. Fluorescence imaging of A549 control cells (control) and cells incubated with conjugates **C1-C3** (at 20 µM for 4 h) (λ_{exc} 350 nm). The signal-to-noise ratio were equal to 23.5 dB, 32.0 dB, 34.5 dB and 36.0 dB for control cells, cells incubated with **C1**, **C2** and **C3**, respectively. Fixed color bar (0-7500 a.u.). Scale bar: 10 µm

In cells incubated with the conjugate **C1** with a classical TPP vector, the luminescence signal observed was not significant compared to control cells. This may be explained by (*i*) a poor internalization in these conditions and/or (*ii*) the above-mentioned FRET between **C1** and the Mitotracker, reducing **C1** fluorescence. In contrast, a clear luminescence signal could be detected in the case of the conjugate **C2** compared to control cells. Gaussian maxima shifted from the zero position of dx (red line) were obtained in the Van Steensel method and a mean Pearson coefficient of 0.83 ± 0.04 was calculated, both suggesting a partial overlay of **C2** labeling with the mitochondrial marker. The conjugate **C3** gave a luminescence signal qualitatively stronger than **C2**, with a comparable sub-cellular distribution as shown by the similar results in colocalization methods (mean Pearson coefficient 0.68 ± 0.06, Figure 2 and Figures S12-S16).

The fluorescence studies are consistent with toxicity studies suggesting a cell penetration increasing in the order **C1**<**C2**<**C3**. They show a partial overlay of the labeling of the conjugates with that of the MitoTracker Deep Red, pointing to a partial preferential localization at the mitochondria, particularly for **C2** and **C3** (Figure 3).

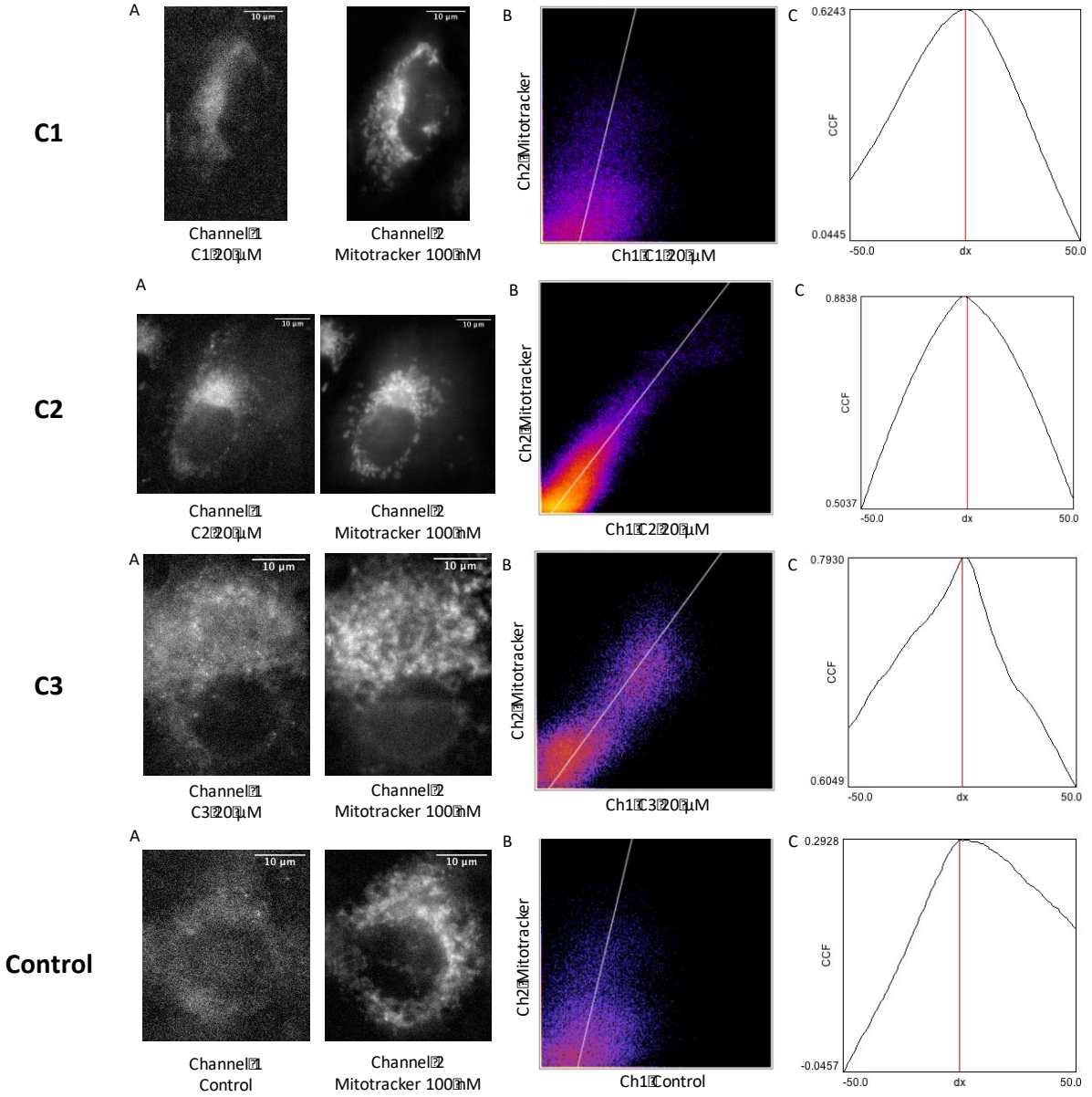

Figure 2. Colocalization analyses with the fluorescence signal of Mitotracker Deep Red. A549 cells were incubated with **C1-C3** probes at 20 µM for 4 hours or without incubation (control). (A) Left: channel 1 - fluorescence image with excitation at λ_{exc} 350 nm, obtained with a gain of 0 over an exposure time of 3s. The signal-to-noise ratio is equal to 17 dB for **C1**, 22 dB for **C2**, 20 dB for **C3** and 12 dB for control cells; Right: channel 2 - fluorescence image of the mitotracker Deep Red (λ_{exc} 644 nm) obtained with a gain of 0 over an exposure time of 5s. (B) Scatter plot or 2D-histogram with a linear regression representing the signal intensity relationship of the two fluorescence images. (C) Van Steensel curve. The cross correlation function is maximal for a shift dx equal to 0, 2, 2 and 1 pixels for **C1**, **C2**, **C3** and control cells, respectively. The Pearson coefficient is equal to 0.62 for **C1**, 0.88 for **C2**, 0.79 for **C3** and 0.30 for control cells**.**

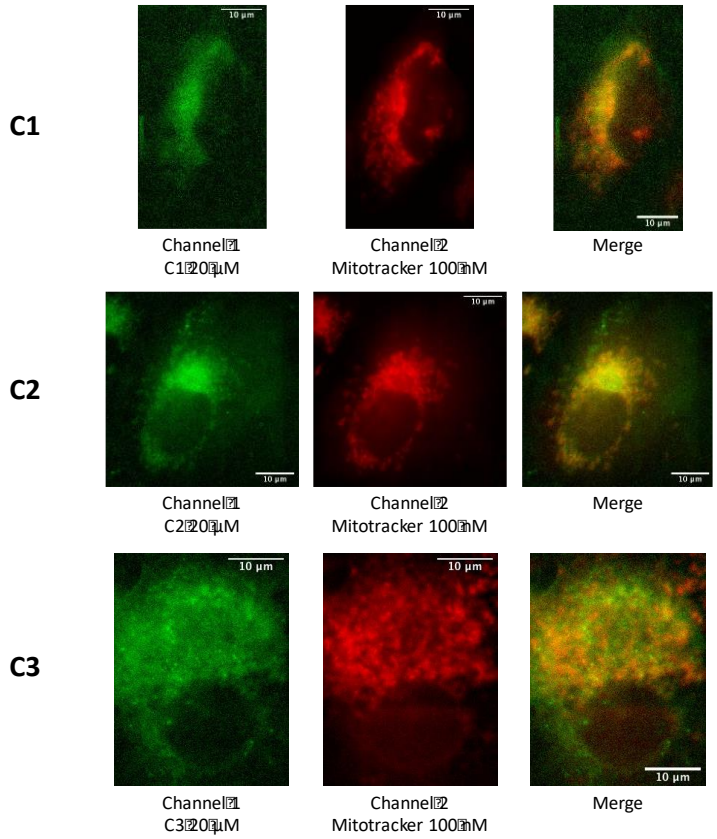

Figure 3. A549 cells were incubated with **C1-C3** probes (20 µM, 4 h). Left: fluorescence signal of the conjugate (λ_{exc} 350 nm); middle: fluorescence signal of Mitotracker Deep Red (λ_{exc} 644 nm); right: merge of conjugate (green) and Mitotracker Deep Red (red) with their overlay in yellow.

Synchrotron radiation scanning X-ray fluorescence nano-imaging (SXRF)

SXRF was used to study the intracellular distribution of rhenium in A549 cells incubated with the probes (20 µM for 4 hours). The cells were seeded on Si_3N_4 silicon nitride membranes, fixed with 4% paraformaldehyde and air-dried (see SI). Chemical fixation and air drying could be used here, the focus of the study not being endogenous metals that can diffuse upon this treatment.[34, 65] Figure 4 shows the elemental distributions of calcium, phosphorus, zinc and rhenium in a single incubated A549 cell (see SI Figure S16-S26 for the mapping of other incubated cells and control cells). In order to avoid spectral overlapping between the Zn-Kα and Re-Lα (~8.6 keV) XRF lines, we use the Zn-Kβ (~9.6 keV) and Re Lß (~10.15 and 10.28 keV) spectral lines to produce the Re and the Zn distribution maps[34] (see SI). The localization of the nucleus is indicated by the phosphorus and zinc mapping. As rhenium is an ultratrace element in biological samples,[36] the rhenium signal can therefore be attributed to the conjugates **C1-C3**.

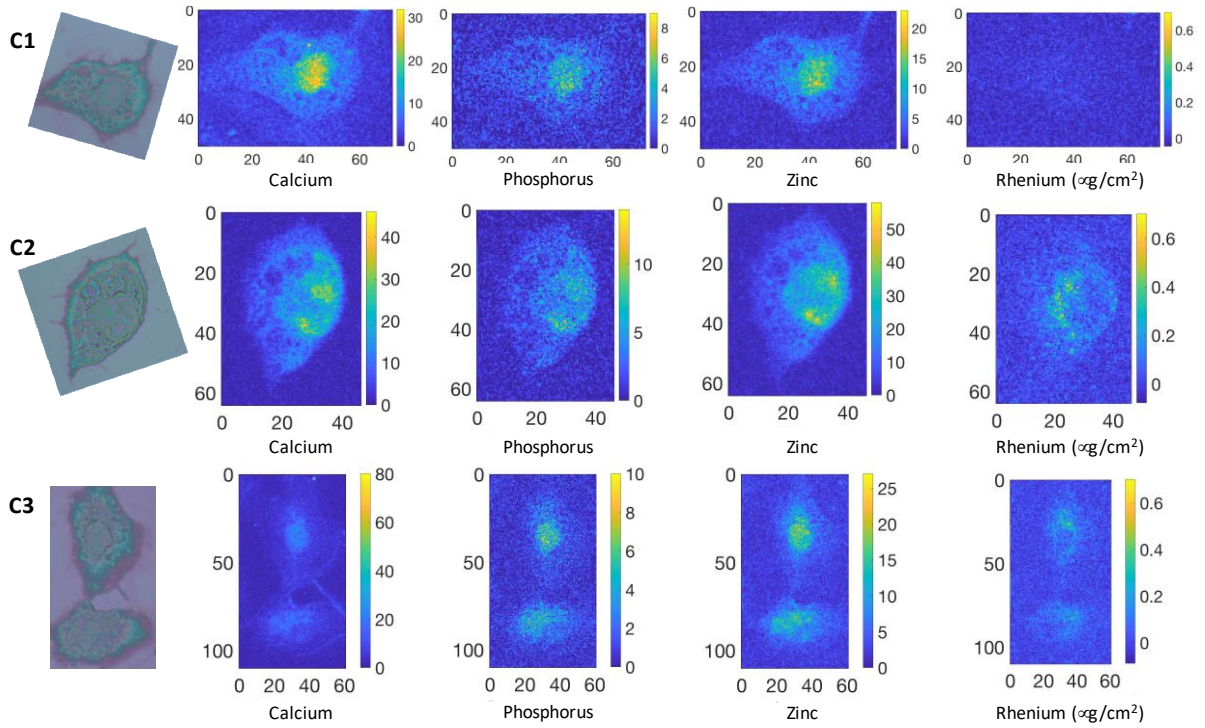

Figure 4. Transmission optical microscope images (left) and elemental distributions of Ca, P, Re, and Zn in A459 cells incubated with **C1-C3** (with color coded map (intensity) (right)). The phosphorus (P), and zinc (Zn) maps, are used to identify the nucleus area. Re was mapped using the Lß lines. A459 cells were incubated for 4 hours with **C1-C3** (20 μM) before fixation and air-drying (excitation at 14 keV; integration time, 300 ms per pixel; pixel size, 500 nm). Scale axis in μm.

Rhenium could not be significantly detected in cells incubated with **C1** (Figures 4 and S16-S18 in comparison to control cells (Figures S24-S26). By contrast, the probes **C2** and **C3** can be unambiguously detected in incubated cells. They show a perinuclear and punctuate distribution that qualitatively matches that observed by fluorescence imaging.

Finally, the amount of rhenium in cells incubated with the three conjugates **C1-C3** was quantified by XRF using a rhenium standard (see SI). The average concentrations expressed in μg per cell are shown in Figure 5. A differential accumulation of the probes in cells in the order **C1** < **C2** < **C3** was confirmed. The amount of **C1** was not significant compared to control cells. The average amount of rhenium in cells incubated with **C2** and **C3** was 4.00 10^{-7} μg per cell and 1.01 10^{-6} μg per cell, respectively, indicating a more than 2-fold increase in cellular accumulation for the **C3** conjugate.

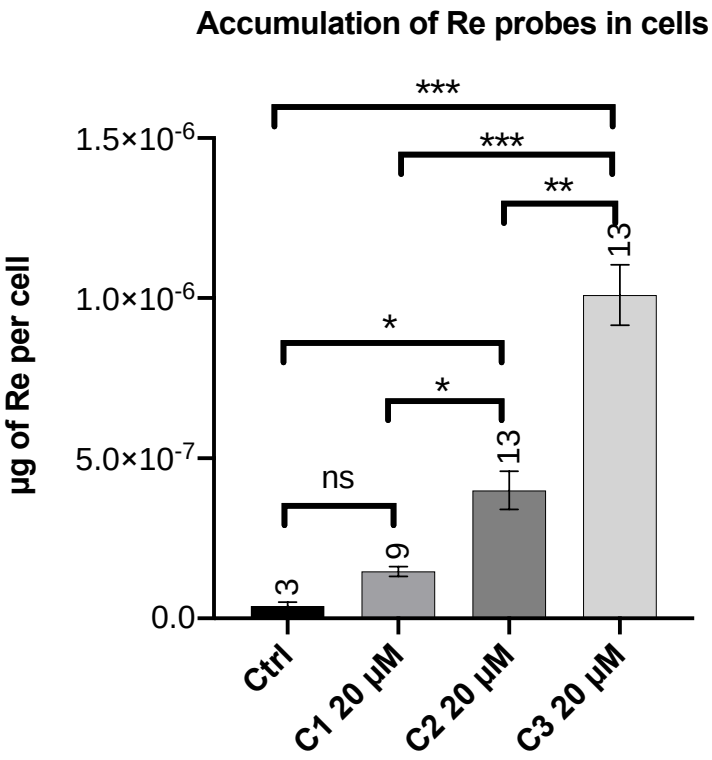

Figure 5. Quantification of rhenium accumulation in cells by X-ray fluorescence. A549 cells were incubated in presence of the rhenium probes **C1-C3** at 20 µM for 4 h. Data represent mean ± SEM. The number of measurements is indicated above each column. The p-values were calculated from the Kruskal-Wallis test (non-parametric ANOVA test) using Prism software. Each comparison stands alone. (***) $p < 0.001$, (**) $p < 0.002$ and (*) $p < 0.033$ and ns means non-significant.

Conclusions

We designed and synthesized rhenium pyta tricarbonyl complexes with triphenylphosphonium cation derivatives as mitochondria targeting probes. The classical TPP^+ was evaluated along with two poly-methylated derivatives TP^*P^+ that were proposed as valuable alternative for mitochondria accumulation.[56-57] The appendage of the non-polar methyl groups enhances the cation's lipophilicity while increasing its solvent accessible surface area and molecular volume, suggested as a key parameter to predict targeting ability. The conjugates displayed typical photophysical properties of rhenium carbonyl complexes with a MLCT absorption band centered at 330 nm and an emission at 530 nm with low quantum yields below 1% in acetonitrile. An increasing toxicity on A549 cells was observed with the lipophilicity of the conjugates, the **C3** complex with a bis-methyl TP^*P^+ being the more toxic with an IC_{50} of 46 µM, still suitable for bioimaging. Fluorescence imaging studies in fixed A549 cells and colocalization studies showed a partial localization at the mitochondria for TP^*P^+ conjugates **C2** and **C3** while no significant signal was observed for TPP^+ complex **C1** when co-incubated with a Mitotracker. The conjugates were finally

mapped in fixed dried cells and quantified using XRF spectroscopy. Compared to **C1**, TP*P$^+$ conjugates **C2** and **C3** were unambiguously detected in incubated single cells with a perinuclear accumulation of punctuate appearance consistent with a partial mitochondrial localization. A higher penetration and accumulation in cells was confirmed with the use of TP*P$^+$ cations, with twice as much bis-methyl cation **C3** compared to mono methyl cation **C2**. Our study expands the use of this alternative family of mitochondria targeting agents and further supports its potential for enhanced mitochondrial therapies. Besides, we identify two Re tricarbonyl complexes as multimodal imaging probes targeting mitochondria as observed by fluorescence and X-ray fluorescence spectroscopies. These probes are a very convenient alternative to immunolabeling involving gold-modified secondary antibodies and compatible with chemical fixation and air drying easily applied for SXRF. Further studies are underway to further demonstrate mitochondrial localization in live cells and in cryofixed samples. Finally, this paves the way towards the development and applications of organelle specific XRF molecular probes that would undoubtedly bring invaluable insights in medicinal inorganic chemistry approaches.

Acknowledgments

We thank IPV doctoral program (Sorbonne Université) for GS's PhD fellowship and École Normale Supérieure for LH's PhD fellowship. CNRS is acknowledged for HB delegation to Singapore. We thank the Fondation pour la Recherche Médicale for financial support (contract DIE20151234413, call « Pionniers de la recherche, Etudes physico-chimiques innovantes pour la biologie et la médecine). We thank Institut Curie (UMR9187, F. Poyer and F. Mahuteau-Betzer) for providing A549 cells. We thank Z. Gueroui (ENS chemistry department) for useful discussions and help with fluorescence microscopy. F.G. would like to thank A*STAR AME IRG A1783c0003, NTU for a start-up grant (M4080552) and MOE Tier 1 grants (RG 11/15 and RG 113/16) for financial support. H.C. would like to thank NTU for NPGS scholarship.

ORCID

Gabrielle Schanne: 0000-0002-8601-1485

Andrea Somogyi: 0000-0002-3814-4152

Kadda Medjoubi: 0000-0003-3352-3820

Nicolas Delsuc: 0000-0001-5570-8311

Clotilde Policar: 0000-0003-0255-1650

Felipe García: 0000-0002-9605-3611

Helene C Bertrand: 0000-0002-3841-022X

References

1. Zheng, N.; Tsai, H. N.; Zhang, X.; Rosania, G. R., The Subcellular Distribution of Small Molecules: From Pharmacokinetics to Synthetic Biology. *Mol. Pharmaceutics* **2011,** *8* (5), 1619-1628.
2. Haughland, R. P., *The Molecular Probes Handbook: A Guide to Fluorescent Probes and Labeling Technologies*. Carlsbad, CA, 2010.
3. Ueno, T.; Nagano, T., Fluorescent probes for sensing and imaging. *Nature Methods* **2011,** *8*, 642-645.
4. Zhu, H.; Fan, J.; Du, J.; Peng, X., Fluorescent Probes for Sensing and Imaging within Specific Cellular Organelles. *Acc. Chem. Res.* **2016,** *49* (10), 2115-2126.
5. Clède, S.; Lambert, F.; Saint-Fort, R.; Plamont, M.-A.; Bertrand, H.; Vessières, A.; Policar, C., Influence of the Side-Chain Length on the Cellular Uptake and the Cytotoxicity of Rhenium Triscarbonyl Derivatives: A Bimodal Infrared and Luminescence Quantitative Study. *Chem. A Eur. J.* **2014,** *20* (28), 8714-8722.
6. Yang, Z.; Cao, J.; He, Y.; Yang, J. H.; Kim, T.; Peng, X.; Kim, J. S., Macro-/micro-environment-sensitive chemosensing and biological imaging. *Chem. Soc. Rev.* **2014,** *43* (13), 4563-4601.
7. Horobin, R. W.; Rashid-Doubell, F.; Pediani, J. D.; Milligan, G., Predicting small molecule fluorescent probe localization in living cells using QSAR modeling. 1. Overview and models for probes of structure, properties and function in single cells. *Biotech. Histochem.* **2013,** *88* (8), 440-460.
8. Králová, J.; Jurášek, M.; Mikšátková, L.; Marešová, A.; Fähnrich, J.; Cihlářová, P.; Drašar, P.; Bartůněk, P.; Král, V., Influence of fluorophore and linker length on the localization and trafficking of fluorescent sterol probes. *Sci. Rep.* **2020,** *10* (1), 22053.
9. McRae, R.; Bagchi, P.; Sumalekshmy, S.; Fahrni, C. J., In Situ Imaging of Metals in Cells and Tissues. *Chem. Rev.* **2009,** *109* (10), 4780-4827.
10. Antony, S.; Aitken, J. B.; Vogt, S.; Lai, B.; Brown, T.; Spiccia, L.; Harris, H. H., X-ray fluorescence imaging of single human cancer cells reveals that the N-heterocyclic ligands of iodinated analogues of ruthenium anticancer drugs remain coordinated after cellular uptake. *J. Biol. Inorg. Chem.* **2013,** *18* (7), 845-853.
11. Hall, M. D.; Dillon, C. T.; Zhang, M.; Beale, P.; Cai, Z.; Lai, B.; Stampfl, A. P. J.; Hambley, T. W., The cellular distribution and oxidation state of platinum(II) and platinum(IV) antitumour complexes in cancer cells. *J. Biol. Inorg. Chem.* **2003,** *8* (7), 726-732.
12. Mathieu, E.; Bernard, A.-S.; Quévrain, E.; Zoumpoulaki, M.; Iriart, S.; Lung-Soong, C.; Lai, B.; Medjoubi, K.; Henry, L.; Nagarajan, S.; Poyer, F.; Scheitler, A.; Ivanović-Burmazović, I.; Marco, S.; Somogyi, A.; Seksik, P.; Delsuc, N.; Policar, C., Intracellular location matters: rationalization of the anti-inflammatory activity of a manganese(ii) superoxide dismutase mimic complex. *Chem. Commun.* **2020,** *56* (57), 7885-7888.

13. Morrison, D. E.; Aitken, J. B.; de Jonge, M. D.; Ioppolo, J. A.; Harris, H. H.; Rendina, L. M., High mitochondrial accumulation of new gadolinium(iii) agents within tumour cells. *Chem. Commun.* **2014,** *50* (18), 2252-2254.
14. Sanchez-Cano, C.; Gianolio D Fau - Romero-Canelon, I.; Romero-Canelon I Fau - Tucoulou, R.; Tucoulou R Fau - Sadler, P. J.; Sadler, P. J., Nanofocused synchrotron X-ray absorption studies of the intracellular redox state of an organometallic complex in cancer cells. *Chem. Commun.* **2019,** *55*, 7065-7068.
15. Sanchez-Cano, C.; Romero-Canelón, I.; Yang, Y.; Hands-Portman, I. J.; Bohic, S.; Cloetens, P.; Sadler, P. J., Synchrotron X-Ray Fluorescence Nanoprobe Reveals Target Sites for Organo-Osmium Complex in Human Ovarian Cancer Cells. *Chem. Eur. J.* **2017,** *23* (11), 2512-2516.
16. McRae, R.; Lai, B.; Fahrni, C. J., Subcellular redistribution and mitotic inheritance of transition metals in proliferating mouse fibroblast cells. *Metallomics* **2013,** *5* (1), 52-61.
17. Carmona, A.; Devès, G.; Roudeau, S.; Cloetens, P.; Bohic, S.; Ortega, R., Manganese Accumulates within Golgi Apparatus in Dopaminergic Cells as Revealed by Synchrotron X-ray Fluorescence Nanoimaging. *ACS Chem. Neurosci.* **2010,** *1* (3), 194-203.
18. Conesa, J. J.; Carrasco, A. C.; Rodríguez-Fanjul, V.; Yang, Y.; Carrascosa, J. L.; Cloetens, P.; Pereiro, E.; Pizarro, A. M., Unambiguous Intracellular Localization and Quantification of a Potent Iridium Anticancer Compound by Correlative 3D Cryo X-Ray Imaging. *Angew. Chem. Int. Ed.* **2020,** *59* (3), 1270-1278.
19. Fus, F.; Yang, Y.; Lee, H. Z. S.; Top, S.; Carriere, M.; Bouron, A.; Pacureanu, A.; da Silva, J. C.; Salmain, M.; Vessières, A.; Cloetens, P.; Jaouen, G.; Bohic, S., Intracellular Localization of an Osmocenyl-Tamoxifen Derivative in Breast Cancer Cells Revealed by Synchrotron Radiation X-ray Fluorescence Nanoimaging. *Angew. Chem. Int. Ed.* **2019,** *58* (11), 3461-3465.
20. Serpell, C. J.; Rutte, R. N.; Geraki, K.; Pach, E.; Martincic, M.; Kierkowicz, M.; De Munari, S.; Wals, K.; Raj, R.; Ballesteros, B.; Tobias, G.; Anthony, D. C.; Davis, B. G., Carbon nanotubes allow capture of krypton, barium and lead for multichannel biological X-ray fluorescence imaging. *Nat. Commun.* **2016,** *7* (1), 13118.
21. Roudeau, S.; Carmona, A.; Perrin, L.; Ortega, R., Correlative organelle fluorescence microscopy and synchrotron X-ray chemical element imaging in single cells. *Anal. Bioanal. Chem.* **2014,** *406* (27), 6979-6991.
22. Suárez, V. T.; Gallet, B.; Chevallet, M.; Jouneau, P.-H.; Tucoulou, R.; Veronesi, G.; Deniaud, A., Correlative transmission electron microscopy and high-resolution hard X-ray fluorescence microscopy of cell sections to measure trace elements concentrations at the organelle level. *bioRxiv* 2020.11.21.392738.
23. Matsuyama, S.; Shimura, M.; Mimura, H.; Fujii, M.; Yumoto, H.; Sano, Y.; Yabashi, M.; Nishino, Y.; Tamasaku, K.; Ishikawa, T.; Yamauchi, K., Trace element mapping of a single cell using a hard x-ray nanobeam focused by a Kirkpatrick-Baez mirror system. *X-Ray Spectrom.* **2009,** *38* (2), 89-94.
24. McRae, R.; Lai, B.; Vogt, S.; Fahrni, C. J., Correlative microXRF and optical immunofluorescence microscopy of adherent cells labeled with ultrasmall gold particles. *J. Struct. Biol.* **2006,** *155* (1), 22-29.
25. Clède, S.; Policar, C., Metal–Carbonyl Units for Vibrational and Luminescence Imaging: Towards Multimodality. *Chem. Eur. J.* **2015,** *21* (3), 942-958.
26. Coogan, M. P.; Fernández-Moreira, V., Progress with, and prospects for, metal complexes in cell imaging. *Chem. Commun.* **2014,** *50* (4), 384-399.
27. Lo, K. K.-W., Molecular Design of Bioorthogonal Probes and Imaging Reagents Derived from Photofunctional Transition Metal Complexes. *Acc. Chem. Res.* **2020,** *53* (1), 32-44.

28. Gillam, T. A.; Sweetman, M. J.; Bader, C. A.; Morrison, J. L.; Hayball, J. D.; Brooks, D. A.; Plush, S. E., Bright lights down under: Metal ion complexes turning the spotlight on metabolic processes at the cellular level. *Coord. Chem. Rev.* **2018,** *375*, 234-255.
29. Hostachy, S.; Policar, C.; Delsuc, N., Re(I) carbonyl complexes: Multimodal platforms for inorganic chemical biology. *Coord. Chem. Rev.* **2017,** *351*, 172-188.
30. Clède, S.; Delsuc, N.; Laugel, C.; Lambert, F.; Sandt, C.; Baillet-Guffroy, A.; Policar, C., An easy-to-detect nona-arginine peptide for epidermal targeting. *Chem. Commun.* **2015,** *51* (13), 2687-2689.
31. Clède, S.; Lambert, F.; Sandt, C.; Gueroui, Z.; Réfrégiers, M.; Plamont, M.-A.; Dumas, P.; Vessières, A.; Policar, C., A rhenium tris-carbonyl derivative as a single core multimodal probe for imaging (SCoMPI) combining infrared and luminescent properties. *Chem. Commun.* **2012,** *48* (62), 7729-7731.
32. Clède, S.; Lambert, F.; Sandt, C.; Kascakova, S.; Unger, M.; Harté, E.; Plamont, M.-A.; Saint-Fort, R.; Deniset-Besseau, A.; Gueroui, Z.; Hirschmugl, C.; Lecomte, S.; Dazzi, A.; Vessières, A.; Policar, C., Detection of an estrogen derivative in two breast cancer cell lines using a single core multimodal probe for imaging (SCoMPI) imaged by a panel of luminescent and vibrational techniques. *Analyst* **2013,** *138* (19), 5627-5638.
33. Henry, L.; Delsuc, N.; Laugel, C.; Lambert, F.; Sandt, C.; Hostachy, S.; Bernard, A.-S.; Bertrand, H. C.; Grimaud, L.; Baillet-Guffroy, A.; Policar, C., Labeling of Hyaluronic Acids with a Rhenium-tricarbonyl Tag and Percutaneous Penetration Studied by Multimodal Imaging. *Bioconj. Chem.* **2018,** *29* (4), 987-991.
34. Hostachy, S.; Masuda, M.; Miki, T.; Hamachi, I.; Sagan, S.; Lequin, O.; Medjoubi, K.; Somogyi, A.; Delsuc, N.; Policar, C., Graftable SCoMPIs enable the labeling and X-ray fluorescence imaging of proteins. *Chem. Sci.* **2018,** *9* (19), 4483-4487.
35. Wedding, J. L.; Harris, H. H.; Bader, C. A.; Plush, S. E.; Mak, R.; Massi, M.; Brooks, D. A.; Lai, B.; Vogt, S.; Werrett, M. V.; Simpson, P. V.; Skelton, B. W.; Stagni, S., Intracellular distribution and stability of a luminescent rhenium(i) tricarbonyl tetrazolato complex using epifluorescence microscopy in conjunction with X-ray fluorescence imaging. *Metallomics* **2017,** *9* (4), 382-390.
36. Rodushkin, I.; Engström, E.; Stenberg, A.; Baxter, D. C., Determination of low-abundance elements at ultra-trace levels in urine and serum by inductively coupled plasma–sector field mass spectrometry. *Anal. Bioanal. Chem.* **2004,** *380* (2), 247-257.
37. Rajendran, L.; Hj, K.; Simons, K., Subcellular targeting strategies for drug design and delivery. *Nat. Rev. Drug Discov.* **2010,** *9*, 29-42.
38. Sakhrani, N. M.; Padh, H., Organelle targeting: third level of drug targeting. *Drug Des Devel Ther* **2013,** *7*, 585-599.
39. Xu, Z.; Xu, L., Fluorescent probes for the selective detection of chemical species inside mitochondria. *Chem. Commun.* **2016,** *52* (6), 1094-1119.
40. Di Lisa, F.; Kaludercic, N.; Carpi, A.; Menabò, R.; Giorgio, M., Mitochondria and vascular pathology. *Pharmacol. Rep.* **2009,** *61* (1), 123-130.
41. Frantz, M.-C.; Wipf, P., Mitochondria as a target in treatment. *Environ. Mol. Mutagen.* **2010,** *51* (5), 462-475.
42. Haelterman, N. A.; Yoon, W. H.; Sandoval, H.; Jaiswal, M.; Shulman, J. M.; Bellen, H. J., A Mitocentric View of Parkinson's Disease. *Ann. Rev. Neurosci.* **2014,** *37* (1), 137-159.
43. Smith, R. A.; Hartley, R. C.; Murphy, M. P., Mitochondria-targeted small molecule therapeutics and probes. *Antioxid Redox Signal* **2011,** *15* (12), 3021-3038.

44. Yousif, L. F.; Stewart, K. M.; Kelley, S. O., Targeting Mitochondria with Organelle-Specific Compounds: Strategies and Applications. *ChemBioChem* **2009,** *10* (12), 1939-1950.
45. Horton, K. L.; Stewart, K. M.; Fonseca, S. B.; Guo, Q.; Kelley, S. O., Mitochondria-penetrating peptides. *Chem Biol* **2008,** *15* (4), 375-382.
46. Kim, S.; Nam, H. Y.; Lee, J.; Seo, J., Mitochondrion-Targeting Peptides and Peptidomimetics: Recent Progress and Design Principles. *Biochemistry* **2020,** *59* (3), 270-284.
47. Zhao, K.; Zhao, G.-M.; Wu, D.; Soong, Y.; Birk, A. V.; Schiller, P. S.; Szeto, H. H., Cell-permeable peptide antioxidants targeted to inner mitochondrial membrane inhibit mitochondrial swelling, oxidative cell death, and reperfusion injury. *J. Biol. Chem.* **2004,** *279* (33), 34682-34690.
48. Smith, R. A. J.; Porteous, C. M.; Gane, A. M.; Murphy, M. P., Delivery of bioactive molecules to mitochondria *in vivo*. *Proc. Nat. Acad. Sci.* **2003,** *100* (9), 5407.
49. Zielonka, J.; Joseph, J.; Sikora, A.; Hardy, M.; Ouari, O.; Vasquez-Vivar, J.; Cheng, G.; Lopez, M.; Kalyanaraman, B., Mitochondria-Targeted Triphenylphosphonium-Based Compounds: Syntheses, Mechanisms of Action, and Therapeutic and Diagnostic Applications. *Chem. Rev.* **2017,** *117* (15), 10043-10120.
50. Murphy, M. P., Slip and leak in mitochondrial oxidative phosphorylation. *Biochim. Biophys. Acta - Bioenergetics* **1989,** *977* (2), 123-141.
51. Qiu, K.; Chen, Y.; Rees, T. W.; Ji, L.; Chao, H., Organelle-targeting metal complexes: From molecular design to bio-applications. *Coord. Chem. Rev.* **2019,** *378*, 66-86.
52. Amoroso, A. J.; Arthur, R. J.; Coogan, M. P.; Court, J. B.; Fernández-Moreira, V.; Hayes, A. J.; Lloyd, D.; Millet, C.; Pope, S. J. A., 3-Chloromethylpyridyl bipyridine fac-tricarbonyl rhenium: a thiol-reactive luminophore for fluorescence microscopy accumulates in mitochondria. *New J. Chem.* **2008,** *32* (7), 1097-1102.
53. Louie, M.-W.; Liu, H.-W.; Lam, M. H.-C.; Lam, Y.-W.; Lo, K. K.-W., Luminescent Rhenium(I) Polypyridine Complexes Appended with an α-D-Glucose Moiety as Novel Biomolecular and Cellular Probes. *Chem. Eur. J.* **2011,** *17* (30), 8304-8308.
54. Skiba, J.; Bernaś, T.; Trzybiński, D.; Woźniak, K.; Ferraro, G.; Marasco, D.; Merlino, A.; Shafikov, M. Z.; Czerwieniec, R.; Kowalski, K., Mitochondria Targeting with Luminescent Rhenium(I) Complexes. . *Molecules* **2017,** *22* (5), 809.
55. Ye, R.-R.; Tan, C.-P.; Chen, M.-H.; Hao, L.; Ji, L.-N.; Mao, Z.-W., Mono- and Dinuclear Phosphorescent Rhenium(I) Complexes: Impact of Subcellular Localization on Anticancer Mechanisms. *Chem. Eur. J.* **2016,** *22* (23), 7800-7809.
56. Hu, Z.; Sim, Y.; Kon, O. L.; Ng, W. H.; Ribeiro, A. J. M.; Ramos, M. J.; Fernandes, P. A.; Ganguly, R.; Xing, B.; García, F.; Yeow, E. K. L., Unique Triphenylphosphonium Derivatives for Enhanced Mitochondrial Uptake and Photodynamic Therapy. *Bioconj. Chem.* **2017,** *28* (2), 590-599.
57. Ong, H. C.; Hu, Z.; Coimbra, J. T. S.; Ramos, M. J.; Kon, O. L.; Xing, B.; Yeow, E. K. L.; Fernandes, P. A.; García, F., Enabling Mitochondrial Uptake of Lipophilic Dications Using Methylated Triphenylphosphonium Moieties. *Inorg. Chem.* **2019,** *58* (13), 8293-8299.
58. Bertrand, H. C.; Clède, S.; Guillot, R.; Lambert, F.; Policar, C., Luminescence modulations of rhenium tricarbonyl complexes induced by structural variations. *Inorg. Chem.* **2014,** *53* (12), 6204-6223.
59. Ching, H. Y. V.; Wang, X.; He, M.; Perujo Holland, N.; Guillot, R.; Slim, C.; Griveau, S.; Bertrand, H. C.; Policar, C.; Bedioui, F.; Fontecave, M., Rhenium Complexes Based on 2-Pyridyl-1,2,3-triazole Ligands: A New Class of CO2 Reduction Catalysts. *Inorg. Chem.* **2017,** *56* (5), 2966-2976.

60. He, M.; Ching, H. Y. V.; Policar, C.; Bertrand, H. C., Rhenium tricarbonyl complexes with arenethiolate axial ligands. *New J. Chem.* **2018,** *42* (14), 11312-11323.
61. Antonenko, Y. N.; Denisov, S. S.; Silachev, D. N.; Khailova, L. S.; Jankauskas, S. S.; Rokitskaya, T. I.; Danilina, T. I.; Kotova, E. A.; Korshunova, G. A.; Plotnikov, E. Y.; Zorov, D. B., A long-linker conjugate of fluorescein and triphenylphosphonium as mitochondria-targeted uncoupler and fluorescent neuro- and nephroprotector. *Biochim. Biophys. Acta - General Subjects* **2016,** *1860* (11, Part A), 2463-2473.
62. Asin-Cayuela, J.; Manas, A.-R. B.; James, A. M.; Smith, R. A. J.; Murphy, M. P., Fine-tuning the hydrophobicity of a mitochondria-targeted antioxidant. *FEBS Lett.* **2004,** *571* (1-3), 9-16.
63. Rokitskaya, T. I.; Murphy, M. P.; Skulachev, V. P.; Antonenko, Y. N., Ubiquinol and plastoquinol triphenylphosphonium conjugates can carry electrons through phospholipid membranes. *Bioelectrochemistry* **2016,** *111*, 23-30.
64. Coogan, M. P.; Fernández-Moreira, V.; Hess, J. B.; Pope, S. J. A.; Williams, C., Rhenium fac-tricarbonyl bisimine complexes: luminescence modulation by hydrophobically driven intramolecular interactions. *New J. Chem.* **2009,** *33* (5), 1094-1099.
65. Jin, Q.; Paunesku, T.; Lai, B.; Gleber, S. C.; Chen, S. I.; Finney, L.; Vine, D.; Vogt, S.; Woloschak, G.; Jacobsen, C., Preserving elemental content in adherent mammalian cells for analysis by synchrotron-based x-ray fluorescence microscopy. *J. Microsc.* **2017,** *265* (1), 81-93.